Ferromagnetism versus charge ordering in the $Pr_{0.5}Ca_{0.5}MnO_3$ and $La_{0.5}Ca_{0.5}MnO_3$ nanocrystals

Z. Jirák,* E. Hadová, O. Kaman, K. Knížek, M. Maryško, and E. Pollert
Institute of Physics, Czech Academy of Sciences, Cukrovarnická 10, Prague 6, Czech Republic

M. Dlouhá and S. Vratislav
Faculty of Nuclear Sciences and Physical Engineering, Czech Technical University, Břehová 7, Prague 1, Czech Republic

(Received 20 August 2009; revised manuscript received 22 October 2009; published 8 January 2010)

The half-doped perovskite manganites $Pr_{0.5}Ca_{0.5}MnO_3$ and $La_{0.5}Ca_{0.5}MnO_3$ in bulk and nanocrystalline form were structurally studied by x-ray and neutron-diffraction methods. The magnetic properties were probed by dc and ac susceptibilities and by isothermal magnetization measurements. The study shows that the room-temperature *Pbnm* perovskite structure, as concerns the lattice distortion, Mn-O distances, and octahedral tilts, is practically unaffected by the particle size. Nonetheless, the low-temperature structural distortion, characteristic for (long- or short-range) charge and orbital ordering in bulk samples, is not observed for 25 nm particles. The absence of the charge-ordering transition is confirmed also by magnetic data. The different behavior compared to bulk is explained by effects of the particle surface. In the nanocrystalline $Pr_{0.5}Ca_{0.5}MnO_3$, an onset of ferromagnetic (FM) arrangement is observed at ~100 K. At the lowest temperature, the magnetic state of the sample can be characterized as a mixture of particles in the metallic FM state with those in the insulating charge and orbitally disordered phase with frozen spins. There is a possibility to induce a global FM state by external field. The $La_{0.5}Ca_{0.5}MnO_3$ nanocrystals develop FM ordering spontaneously below $T_C=260$ K.

DOI: 10.1103/PhysRevB.81.024403 PACS number(s): 75.47.Lx, 78.67.Bf

I. INTRODUCTION

The manganite perovskites with noninteger valence Mn^{3+}/Mn^{4+} valence exhibit fascinating spectrum of physical properties depending on whether the outermost e_g electrons ($d_{3z^2-r^2}$ and $d_{x^2-y^2}$ orbitals) are localized on individual transition-metal sites or delocalized throughout the solid. The localization is often associated with a preferential occupation of the eigenstates [generally $\sin(\alpha)\cdot d_{3z^2-r^2} \pm \cos(\alpha)\cdot d_{x^2-y^2}$], which leads, via strong lattice-orbital coupling, to the development of a long-range ordered pattern. This phenomenon, referred as orbital ordering, makes the bonding between the cations in the oxides strongly directional. The kind of the occupied orbitals and their mutual orientation govern magnetic interactions and electron transport. If the formal manganese valence is of some rational value, the orbital ordering may coexist with certain Mn^{3+}/Mn^{4+} charge ordering (CO). The prototypical case is the $Mn^{3+}/Mn^{4+}=1:1$ ordering established in the "half-doped" manganites $La_{0.5}Ca_{0.5}MnO_3$ (Refs. 1 and 2) and $Pr_{0.5}Ca_{0.5}MnO_3$ (Refs. 3 and 4) below $T_{CO}=225$ and 245 K, respectively. The onset of the ordering is accompanied with an order of magnitude increase in the resistivity and a change in magnetic interactions from the ferromagnetic (FM) to antiferromagnetic (AFM) ones, manifested by a drop of magnetic susceptibility below T_{CO}. At still lower temperatures, a long-range AFM arrangement of the so-called charge-exchange (CE) type is formed. This AFM ground state is exceptionally robust in $Pr_{0.5}Ca_{0.5}MnO_3$ as concerns the stability in high external magnetic field [up to 150–200 kOe (Ref. 5)]. On the other hand, the $La_{0.5}Ca_{0.5}MnO_3$ compound is very sensitive to the field. This should be related to the metastable (phase separated) state of this compound—there are always some FM charge-disordered regions dispersed in the AFM charge-ordered matrix.[6] Their presence seems to be generic since the FM phase is formed simultaneously with the charge ordering. The $La_{0.5}Ca_{0.5}MnO_3$ samples studied extensively by Radaelli *et al.*[2,7] and Huang *et al.*[8] comprised to 10–20 % of residual FM phase at the lowest temperature but much larger FM amounts are frequently reported depending on sample granularity or defects and cooling regimes.

An interesting phenomenon is the suppression of charge order and development of FM phase with reducing of the crystalline size in the half-doped manganite materials. This was demonstrated first, by means of magnetometry, on samples $La_{0.5}Ca_{0.5}MnO_3$ with decreased grain size down to 180 nm and confirmed later on nanoparticles with size as small as 15 nm.[9,10] Similar destabilization of the charge order and onset of FM correlations was reported very recently also for the $Pr_{0.5}Ca_{0.5}MnO_3$ system in form of nanoparticles with size reduced down to 20 nm.[11] The present work is concerned with a more complex structural and magnetic characterization of the $Pr_{0.5}Ca_{0.5}MnO_3$ and $La_{0.5}Ca_{0.5}MnO_3$ nanosize particles and the bulk materials. By means of x-ray and neutron-diffraction methods, it is demonstrated that the nanosize form does not lead to a substantial change in the crystal structure inside the grains so that the suppression of the charge order and CE-type AFM arrangement in the nanoparticles should be ascribed to the surface effects solely. Without charge and orbital orders, the dominant magnetic interactions in the half-doped manganites arise due to the double exchange $Mn^{3+} \leftrightarrow Mn^{4+}$ resonance and they are isotropic and ferromagnetic. Consistently, the present $La_{0.5}Ca_{0.5}MnO_3$ particles of 25 nm size develop spontaneous FM ordering below $T_C=260$ K. The magnetic state of the $Pr_{0.5}Ca_{0.5}MnO_3$ particles of comparable size is more complex. It behaves as a cluster glass or superparamagnet below ~100 K but global FM state can be induced by external field of few tens kiloersted.

II. EXPERIMENTAL

The nanocrystals of controlled size were prepared using a slightly modified sol-gel precursor route.[12] As a first step, the corresponding amounts of Pr_6O_{11} (or La_2O_3), $CaCO_3$, and $MnCO_3$ were separately dissolved in nitric acid and mixed together with ethylene glycol in a ratio of (0.5[Pr or La] +0.5[Ca]+[Mn])/9.38[ethylene glycol] at pH$\sim$0.8. Further steps included evaporation at 80–90 °C, drying at 180 °C and calcination at 250 °C. The final heating was effectuated at selected temperatures in the range of 600–800 °C for 3 h in air. The phase composition of the products and size of the particles were checked by transmission electron microscopy (TEM) observation and x-ray diffraction analysis (Bruker D8, Cu $K\alpha$, SOL-X energy dispersive detector). The calcinate prepared at 250 °C consisted of purely amorphous matter that was gradually transformed, after heating at 600 °C, to the perovskite phase. No other phases, e.g., hausmannite that would not be possible to dissolve at relatively low temperatures of the final heating, were detected after the thermal treatment in this temperature range. Let us note that this attainment, resulting from a suitably established conditions of the precursor preparation, appeared prerequisite for a successful synthesis of the pure perovskite phase $Pr_{0.5}Ca_{0.5}MnO_3$ of the orthorhombic *Pbnm* symmetry at 700 °C (nanocrystals of the 25 nm size) and 800 °C (40 nm). The $La_{0.5}Ca_{0.5}MnO_3$ nanocrystals were prepared following an analogous precursor route and final heating at 700 °C (25 nm size). The bulk samples of $Pr_{0.5}Ca_{0.5}MnO_3$ and $La_{0.5}Ca_{0.5}MnO_3$ were prepared by sintering of the 25 nm particles at 1200 °C, which resulted in ceramics with large crystalline grains exceeding 1 μm.

The crystal structure determination was done using the Rietveld analysis (program FULLPROF) of x-ray diffraction data. In selected cases the x-ray investigation was performed at 90 K, as well. More detailed structural study was undertaken on the 25 nm nanocrystals $Pr_{0.5}Ca_{0.5}MnO_3$ and $La_{0.5}Ca_{0.5}MnO_3$ by means of neutron diffraction at apparatus KSN-2 in Rez near Prague. The experiments were done at the room and liquid-helium temperatures using the neutron wavelength $\lambda=1.369$ Å.

The magnetic measurements over the temperature region 5–300 K were made employing superconducting quantum interference device magnetometers MPMS-5S and MPMS XL (Quantum Design). The zero-field-cooled (ZFC) and field-cooled (FC) dc susceptibilities were measured under applied magnetic fields of 20 and 100 Oe. The hysteresis loops and virgin magnetization curves were recorded at different temperatures using the fields up to 70 kOe. The thermoremanent magnetization (TRM) was measured after cooling the sample from 300 to 5 K in a field $H=3$ Oe. At $T=5$ K, the field was switched off and TRM was recorded during warming the sample with rate of 1 K/min. The ac susceptibility measurements at frequencies 0.04–300 Hz were performed using a driving ac magnetic field $H=3$ Oe for $Pr_{0.5}Ca_{0.5}MnO_3$ and $H=0.5$ Oe for $La_{0.5}Ca_{0.5}MnO_3$. The value of H was chosen in order to remain in the linear region of the dependence $m(H)$. The high-temperature dc susceptibility between 330 and 800 K was measured under applied $H=20$ kOe using the magnetosusceptometer DSM 10 (Manics).

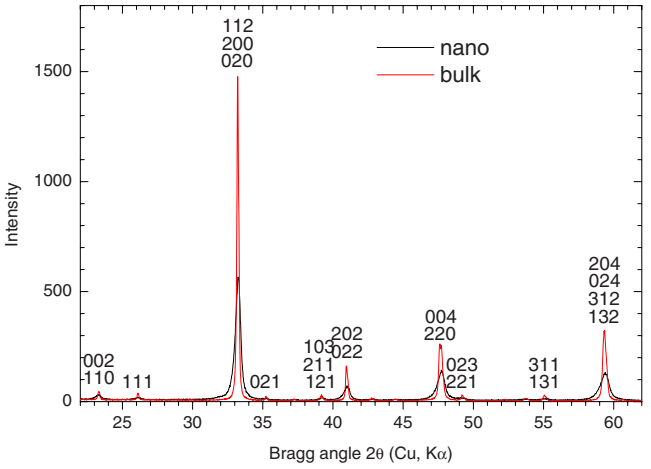

FIG. 1. (Color online) X-ray diffraction pattern of the $Pr_{0.5}Ca_{0.5}MnO_3$ nanoparticles (25 nm size) and bulk (grains exceeding 1 μm).

To make a comparison with manganites exhibiting purely FM ground state, some magnetic experiments on $Pr_{0.5}Ca_{0.5}MnO_3$ and $La_{0.5}Ca_{0.5}MnO_3$ were complemented by measurements on nanoparticles and bulk of the $La_{0.75}Sr_{0.25}MnO_3$ composition. The nanocrystalline material was prepared and previously characterized as reported elsewhere.[13,14] The bulk $La_{0.75}Sr_{0.25}MnO_3$ sample was produced by sintering of the nanoparticles as mentioned above.

III. RESULTS

A. Crystal structure

The x-ray diffraction patterns taken on the nanoparticles prepared at 700 °C and on the pulverized ceramics sintered at 1200 °C are shown in Fig. 1. Based on the observed broadening of diffraction lines, the sizes of the $Pr_{0.5}Ca_{0.5}MnO_3$ and $La_{0.5}Ca_{0.5}MnO_3$ nanoparticles were determined to 25 nm. This value is consistent with TEM pictures that showed round crystalline grains with diameters 17–50 nm, often interconnected by narrow bridges to form agglomerates.

The neutron-diffraction patterns for the nanoparticles are shown in Figs. 2 and 3. There is no obvious difference between the data at 298 and 7 K for $Pr_{0.5}Ca_{0.5}MnO_3$, which shows that there is no or only minor long-range magnetic ordering at the low temperature. Namely, any eventual AFM ordered moments are below $0.2\mu_B$ per Mn ion and the FM ones are below $0.4\mu_B$ per Mn ion at present resolution. On the other hand, for $La_{0.5}Ca_{0.5}MnO_3$ some additional intensity appears at 7 K at diffraction line 110+002 ($2\theta=20.6°$) and 200+020+112 ($2\theta=29.2°$), which is a signature for FM long-range ordering in the sample. The FM moment is refined to $1.7\pm0.2\mu_B$ per Mn ion.

The results of a constrained Rietveld refinement based on the neutron-diffraction and x-ray patterns are summarized in Table I. Here, the orthorhombic *Pbnm* perovskite structure is characterized by the lattice parameters, the Mn-O bonding distances and the average tilt angles Mn-O-Mn. It is seen that the room-temperature data on bulk samples (results of the

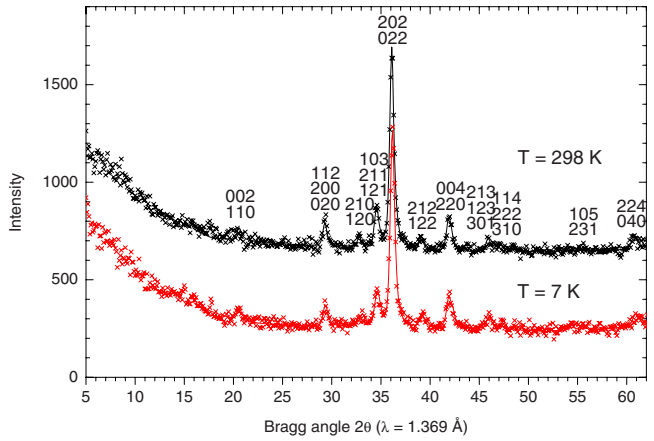

FIG. 2. (Color online) Neutron-diffraction patterns of the $Pr_{0.5}Ca_{0.5}MnO_3$ nanoparticles (25 nm size) at 298 and 7 K. There is no CE-type AFM or FM contribution at $T=7$ K.

x-ray diffraction) agree reasonably well with the reference data for $Pr_{0.5}Ca_{0.5}MnO_3$ (Ref. 4) and $La_{0.5}Ca_{0.5}MnO_3$ (Refs. 2 and 8) that have been determined by much more sensitive high-resolution neutron diffraction. As concerns the structural parameters of the 25 nm particles, there are only subtle differences observed at room temperature. One is a certain increase in the unit-cell volume, which might be caused by some small change in the oxygen stoichiometry compared to the ceramics. The second one concerns the orthorhombic distortion of the samples. The differences between lattice parameters a, b, and $c/\sqrt{2}$ are rather small but there is an additional pseudotetragonal strain in both the $Pr_{0.5}Ca_{0.5}MnO_3$ and $La_{0.5}Ca_{0.5}MnO_3$ nanoparticles, which are clearly outside the experimental uncertainty. This strain is evidenced in Table I by an increase in the a and b parameters, combined with a decrease in the c parameters. Otherwise, the Mn-O distances and octahedral tilts in the *Pbnm* perovskite structure are practically unaffected by the nanosize form. The speculations about the surface tension and large structural distortions (for $La_{0.5}Ca_{0.5}MnO_3$ nanoparticles see, e.g., Ref. 15) are thus disproved. It should be noted that a very recent

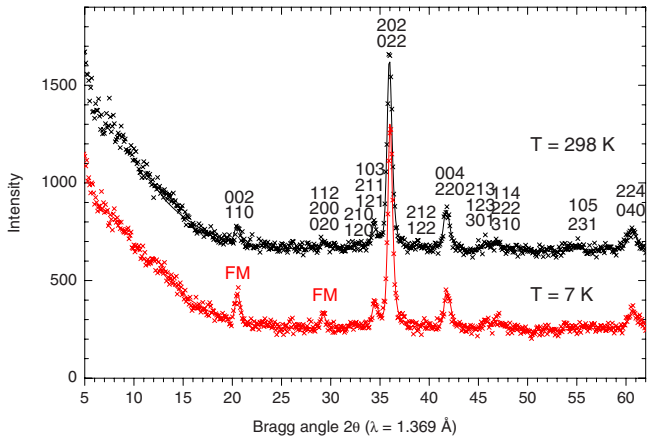

FIG. 3. (Color online) Neutron-diffraction patterns of the $La_{0.5}Ca_{0.5}MnO_3$ nanoparticles (25 nm size) at 298 and 7 K. The presence of long-range FM ordering at $T=7$ K is evidenced by the additional intensity to nuclear lines.

study of the $La_{0.5}Ca_{0.5}MnO_3$ nanoparticles also showed only insignificant changes in lattice parameters upon reducing of grain size.[10]

Despite the similar room-temperature structure, the low-temperature structural data of nanoparticles differ significantly from that of the bulk. It is notoriously known that the onset of charge ordering in half-doped manganites is manifested by a change in the pseudocubic metric of the perovskite lattice ($a \approx b \approx c/\sqrt{2}$ at 300 K) to a tetragonally contracted one ($a \approx b \geq c/\sqrt{2}$). This arises owing to a polarization of the localized e_g orbitals on Mn sites into the *ab* plane and formation of a complex superstructure, which is described in more detail for $Pr_{0.5}Ca_{0.5}MnO_3$ by Jirak *et al.*[4] and Daoud-Aladine *et al.*[16] and for $La_{0.5}Ca_{0.5}MnO_3$ by Radaelli *et al.*[2] It is seen in Table I that also the present bulk sample $Pr_{0.5}Ca_{0.5}MnO_3$ develops upon cooling to low temperature the expected pseudotetragonal contraction and the practically regular MnO_6 octahedra change to strongly distorted ones, quantified by ratio $(\text{Mn-O})_c/\langle(\text{Mn-O})_{ab}\rangle=0.98$. (Only average values of the Mn-O lengths in *ab* plane could be determined in the present constrained refinement.) On the other hand, the 25 nm particles exhibit only very small additional deformation of the lattice upon cooling from 300 to 7 K and the refined Mn-O lengths are unchanged within standard deviations. The conclusion relevant to rejection of any substantial short-range charge ordering in nanoparticles is thus supported by structural results.

B. Magnetic state

The magnetic state of the bulk and noncrystalline samples of $Pr_{0.5}Ca_{0.5}MnO_3$ and $La_{0.5}Ca_{0.5}MnO_3$ was investigated further by the dc magnetic-susceptibility and magnetization measurements (see Fig. 4 and 5). The frequency-dependent ac susceptibility measurements were performed in order to illustrate the dynamic properties of the nonhomogeneous magnetic ground state of the 25 nm nanocrystals. These data are presented below in the next section (see Fig. 8).

The susceptibility data on bulk sample $Pr_{0.5}Ca_{0.5}MnO_3$ in Fig. 4 show a characteristic maximum at the charge-ordering transitions at $T_{CO}=245$ K and indistinct anomaly associated with the transition to the CE-type AFM state at $T_N=165$ K on cooling and 185 K on heating. The low-temperature value of the susceptibility is very low, the increase below ~100 K is due to the paramagnetic contribution of praseodymium ions. As concerns the possibility of FM regions in the sample, we refer to the virgin magnetization curve at $T=5$ K in Fig. 5. It can be approximated by a linear dependence combined with a negligible moment of $\sim 0.005\mu_B$ per Mn. These findings evidence an almost pure charge-ordered AFM ground state in the present bulk sample.

The charge-ordering and AFM anomalies are largely suppressed in the 40 nm nanocrystals and vanish practically in the 25 nm nanocrystals. New feature is a sudden increase in the susceptibility at a cooling below the critical temperature $T_C \sim 100$ K and a large irreversibility in the course of the ZFC and FC susceptibilities below this point (see Fig. 4). The existence of a maximum in the ZFC susceptibility resembles the cluster glass or superparamagnetic state charac-

TABLE I. The structural data summary for bulk and nanoparticles of $Pr_{0.5}Ca_{0.5}MnO_3$ and $La_{0.5}Ca_{0.5}MnO_3$. The parameters refer to the perovskite unit cell of *Pbnm* symmetry.

	a (Å)	b (Å)	c (Å)	$c/\sqrt{2}$ (Å)	V (Å^3)	Mn-O$_c$	⟨Mn-O⟩$_{ab}$	Tilt (deg)	R_p	χ^2
Room temperature										
$Pr_{0.5}Ca_{0.5}MnO_3$ (Ref. 4)	5.3949(1)	5.4042(2)	7.6064(2)	5.3785	221.77(1)	1.937(0)	1.945(1)	158.0(1)		
Large grains >1000 nm	5.3964(1)	5.4046(1)	7.6124(1)	5.3828	222.02(1)	1.941(1)	1.944(5)	157.9(4)	9.96[a]	1.91[a]
Nano 25 nm	5.407(1)	5.408(1)	7.605(1)	5.377	222.36(5)	1.942(2)	1.952(8)	156.6(6)	8.72[a], 5.24[b]	1.45[a], 1.61[b]
$La_{0.5}Ca_{0.5}MnO_3$ (Ref. 2)	5.4355(1)	5.4248(1)	7.6470(2)	5.4072	225.49(1)	1.941(0)	1.945(2)	160.94(7)		
Reference 8	5.4305(2)	5.4220(2)	7.6425(3)	5.4040	225.03(2)	1.940(1)	1.943(5)			
Large grains >1000 nm	5.4275(2)	5.4192(2)	7.6488(2)	5.4085	224.96(1)	1.940(1)	1.942(6)	161.2(4)	11.3[a]	2.25[a]
Nano 25 nm	5.445(2)	5.434(2)	7.637(1)	5.400	225.95(9)	1.937(2)	1.94(1)	161.6(9)	8.30[a], 4.78[b]	2.13[a], 1.10[b]
Low temperatures										
$Pr_{0.5}Ca_{0.5}MnO_3$ T=5 K (Ref. 17)	5.4335(2)	5.4357(2)	7.4831(2)	5.2914	221.01(2)	1.913(0)	1.955(2)	157.3(2)		
Grains >1000 nm T=90 K	5.4328(8)	5.4343(9)	7.4971(4)	5.3013	221.34(5)	1.913(3)	1.95(1)	158.6(18)	7.73[a]	1.57[a]
Nano 25 nm T=90 K	5.396(1)	5.417(1)	7.584(1)	5.363	221.70(8)	1.935(3)	1.95(1)	156.5(12)	5.43[a]	1.32[a]
Nano 25 nm T=7 K	5.407(1)	5.408(1)	7.575(2)	5.356	221.32(9)	1.932(4)	1.947(9)	157.5(7)	5.05[b]	1.54[b]
$La_{0.5}Ca_{0.5}MnO_3$ T=5 K (Ref. 2)	5.4763(3)	5.4466(3)	7.5247(4)	5.3208	224.44(2)	1.915(0)	1.955(1)	160.22(6)		
Reference 8	5.4709(1)	5.4410(3)	7.5187(3)	5.3165	223.81(2)	1.915(1)	1.954(2)			
Nano 25 nm T=7 K	5.437(1)	5.426(1)	7.616(2)	5.385	224.7(1)	1.935(5)	1.94(2)	161.4(16)	5.12[b]	1.25[b]

[a]X-ray diffraction.
[b]Neutron diffraction.

terized by a freezing or blocking temperature T_B. This effect depends on the particle diameter and has, in real case of a polydisperse powder, a finite distribution $f(T_B)$. We attempted to obtain information on the blocking temperature distribution using the relation $f(T_B) \sim d(\chi_{ZFC} - \chi_{FC})/dT$.[18] For the 25 nm nanocrystals the course of $f(T_B)$ can be seen in the left panel of Fig. 6. Let us notice that the distribution $f(T_B)$ remains nonzero up to about 120 K. Below this temperature, the true blocked FM state is formed in the largest nanoparticles, which can be well seen in the temperature dependence of the thermoremanent magnetization in the right panel of Fig. 6, as well as in the above-mentioned increase in the susceptibility (see left panel of Fig. 4). With decreasing temperature the volume corresponding to the blocked FM state increases since the number of the nanoparticles with lower T_B increases following the distribution $f(T_B)$. Due to this effect, the increase in the susceptibility below T_C is not as sharp as it is usually observed in the bulk materials (see the comparison for the doped nanocrystalline and bulk manganites in Fig. 9 below).

The nonuniform magnetic state in the 25 nm nanocrystals $Pr_{0.5}Ca_{0.5}MnO_3$ is manifested further by virgin magnetization curves (see Fig. 5 for selected temperatures). Up to 105 K, two contributions can be identified in lower external fields. The first one is a magnetization proportional to H, which can be ascribed to particles in a charge and orbitally disordered (glassy) state with frozen spins and the second represents a nearly unhysteretic Langevin-type contribution that originates from particles in FM state. At temperatures higher than

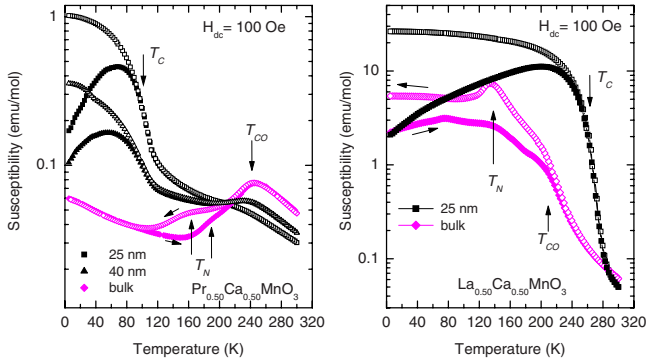

FIG. 4. (Color online) ZFC and FC susceptibilities (in log scale) showing the gradual suppression of the charge-ordering transition and formation of ferromagnetic regions with decreasing size of particles in $Pr_{0.5}Ca_{0.5}MnO_3$ and $La_{0.5}Ca_{0.5}MnO_3$.

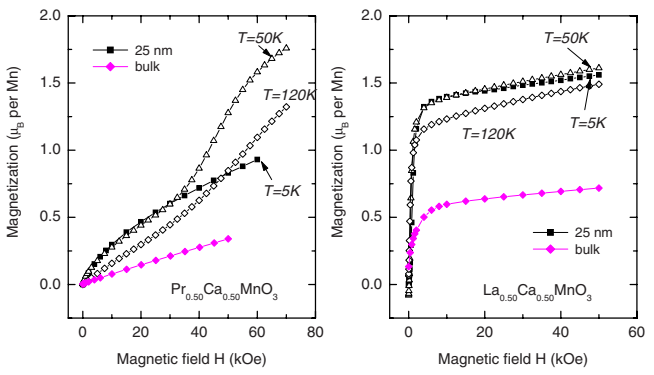

FIG. 5. (Color online) The virgin magnetization curves of $Pr_{0.5}Ca_{0.5}MnO_3$ and $La_{0.5}Ca_{0.5}MnO_3$ nanoparticles (T=5, 50, and 120 K) compared to those for bulk samples (T=5 K).

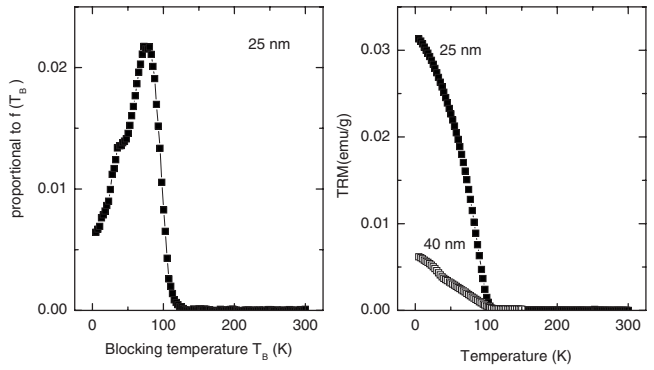

FIG. 6. (Left panel) The distribution of blocking temperatures T_B in the 25 nm particles of $Pr_{0.5}Ca_{0.5}MnO_3$, derived from $d(\chi_{ZFC}-\chi_{FC})/dT$ ($H=20$ Oe). (Right panel) The thermoremanent magnetization in the 25 and 40 nm particles ($H=3$ Oe).

about 80 K this second contribution could be interpreted as a manifestation of an interacting superparamagnet (see Ref. 19) or of a coexistence of the superparamagnetic and blocked FM phases. Below 80 K practically all the superparamagnetic particles develop a blocked FM state. The average FM moment in the $Pr_{0.5}Ca_{0.5}MnO_3$ nanocrystalline sample is estimated from the magnetization curve at $T=5$ K to about $0.2\mu_B$ per Mn only, which is below the sensitivity of our neutron-diffraction experiments. The small moment value suggests that FM state is actually formed only in a minor part of the particles. Another important aspect is the influence of the high magnetic fields ($H>20$ kOe). At $T=5$ K, we observe no change in the magnetic state up to the highest field. When the temperature is increased (see, e.g., the magnetization at 50 K), a relatively modest field of about 50 kOe is able to revert the particles in glassy state with frozen spins to the FM ones. This metamagnetic transition is in a contrast to the very robust charge-ordered ground state in the bulk $Pr_{0.5}Ca_{0.5}MnO_3$ material.[5]

The paramagnetic behavior of the $Pr_{0.5}Ca_{0.5}MnO_3$ bulk and 25 nm particles is illustrated in Fig. 7. After subtraction of a Curie-type paramagnetic contribution for praseodymium,[20] the high-temperature slope of the inverse susceptibility yields the same value $\mu_{eff}=4.51\mu_B$ for both materials, close to the theoretical value $4.42\mu_B$ for the 1:1 mixture of Mn^{3+} and Mn^{4+}. The linear extrapolation gives an intercept (Weiss constant) $\Theta=290$ and 200 K, respectively, pointing to somewhat weaker FM interactions in nanocrystals compared to bulk at elevated temperatures.

In the case of $La_{0.5}Ca_{0.5}MnO_3$, the dc susceptibility for bulk material in Fig. 4 shows the charge-ordering anomaly at $T_{CO}\sim 210$ K and AFM transition at $T_N\sim 140$ K (similar susceptibility data with somewhat higher $T_{CO}=225$ K and $T_N\sim 160$ K are reported for $La_{0.5}Ca_{0.5}MnO_3$ by Radaelli *et al.*[7] and Huang *et al.*[8]). Nonetheless, the high level of the susceptibility ~ 5 emu/mol at the lowest temperatures and FM character of the magnetization curve at $T=5$ K (see Fig. 5) evidence that simultaneously with the charge-ordered phase spontaneous FM regions are formed. The extrapolation to zero field gives an average moment of about $0.6\mu_B$ per Mn. Considering that the theoretical moment is $3.5\mu_B$ for full FM alignment, the value obtained corresponds to 17% of FM phase in the sample.

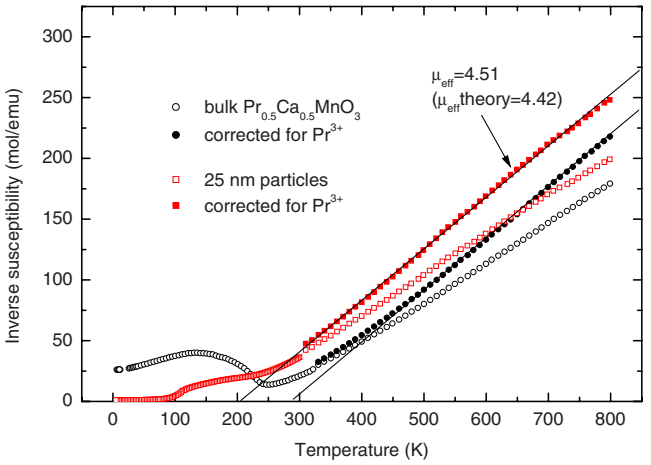

FIG. 7. (Color online) The inverse susceptibility of $Pr_{0.5}Ca_{0.5}MnO_3$ up to 800 K. Red symbols—25 nm particles and black symbols—bulk sample. Full symbols and the linear (Curie-Weiss) approximation are data after the subtraction of the Curie-type paramagnetic contribution for Pr^{3+} ions.

The magnetic properties of 25 nm particles of $La_{0.5}Ca_{0.5}MnO_3$ closely approach the observations on a similar nanocrystalline material studied recently by Rozenberg *et al.*[10] The dc susceptibility in Fig. 4 is characteristic for the formation of a spontaneous FM state with $T_C=260$ K. This is clearly higher than the formation of FM regions in the present bulk sample ($T_C<240$ K, in agreement with $T_C\sim T_{CO}=225$ K reported by Radaelli *et al.*[7]) but close to the T_C found by Huang *et al.*[8] on their $La_{0.5}Ca_{0.5}MnO_3$ bulk sample. The extrapolation of the magnetization data in Fig. 5 to zero field gives an average FM moment of about $1.4\mu_B$ per Mn ion, corresponding to 60% reduction from the saturation value (the theoretical moment is $3.5\mu_B$ for full FM alignment). The long-range ordered moment, derived from the neutron-diffraction data at 7 K (Fig. 3) is $1.7\mu_B$ per Mn ion, which corresponds to about 50% reduction from the saturation value. The remaining volume fraction of the nanocrystalline material is responsible for a large paraprocess seen in Fig. 5 and can be partly or totally attributed to magnetically dead surface layers of the nanocrystals as discussed below.

IV. DISCUSSION

The studied magnetic systems composed of the nanoparticles are inhomogeneous in two aspects. First, though the each particle is of a single-crystal domain there is an important role of the surface. The terminal ions with incomplete coordination number and other surface defects distort by elastic and electric forces the regular periodicity to a significant depth and modify the interatomic exchange interactions. The magnetic arrangement in the outer shell can be thus very different from that in the particle core. For oxides with FM ground state, a model of the magnetic core with nonmagnetic shell is widely accepted. The second aspect is associated with fluctuations of chemical composition, kinetics of the phase transition or the grain-size dispersity, which makes

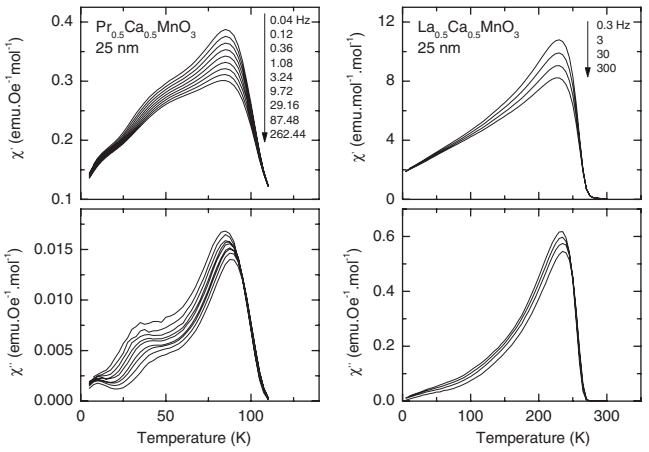

FIG. 8. The real and imaginary parts of the ac susceptibility in the $Pr_{0.5}Ca_{0.5}MnO_3$ and $La_{0.5}Ca_{0.5}MnO_3$ nanoparticles.

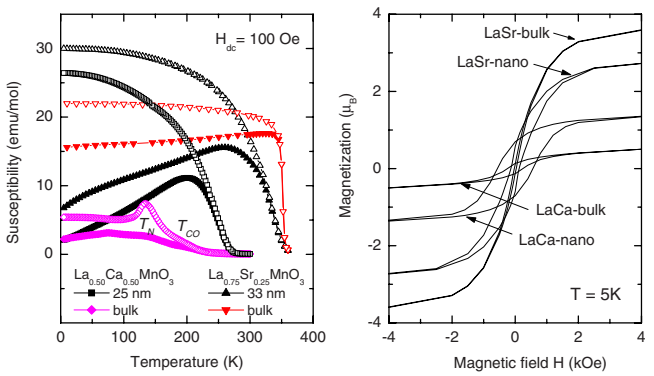

FIG. 9. (Color online) The ZFC (solid symbols) and FC (open symbols) susceptibilities for nanoparticles and bulk samples of $La_{0.5}Ca_{0.5}MnO_3$ and $La_{0.75}Sr_{0.25}MnO_3$. The right panel shows the low-field details of hysteresis loops at 5 K.

possible to stabilize in different particles magnetic states of different types or dynamics.

The experimental data show that both the $Pr_{0.5}Ca_{0.5}MnO_3$ and $La_{0.5}Ca_{0.5}MnO_3$ nanocrystals of the 25 nm sizes exhibit a significant FM response in the external field and the charge ordering is absent. The character of a spontaneous magnetic state is, however, very different for these two compounds. This concerns especially the values of average magnetic moments. It can be estimated from the magnetization curves at $T=5$ K in Fig. 5 that the spontaneous magnetization in $Pr_{0.5}Ca_{0.5}MnO_3$ is about $0.2\mu_B$ per Mn, which means that only a minority of the nanoparticles develop FM state in their cores while majority are in a charge-disordered glassy state with frozen spins. In contrary, the average moment in $La_{0.5}Ca_{0.5}MnO_3$, derived from the neutron-diffraction and magnetization measurements, achieves 1.4 and $1.7\mu_B$ per Mn ion, respectively. The "near FM" character of the $La_{0.5}Ca_{0.5}MnO_3$ sample is reflected also by the low-temperature FC value of the dc susceptibility in Fig. 4, ~25 emu/mol, which is comparable to what is generally observed for bulk FM manganites and is much larger than the value ~1 emu/mol obtained for the $Pr_{0.5}Ca_{0.5}MnO_3$ nanocrystals. Despite of the very different values, the character of the irreversibility of the ZFC and FC curves is similar, suggesting a highly nonuniform magnetic state (broad distribution of the blocking temperatures) in both samples.

The dynamics of the complex magnetic state is manifested in the ac susceptibility in Fig. 8. Both the real and imaginary parts are frequency dependent. Similarly to the dc susceptibility, the absolute values are much larger for $La_{0.5}Ca_{0.5}MnO_3$. For $Pr_{0.5}Ca_{0.5}MnO_3$, a pronounced two-peak feature is observed in the temperature range below 110 K. Let us remark that similar observations concerning the ac susceptibility were reported in the study of Rozenberg *et al.*[21] on the 30 nm particles of the $La_{0.7}Ca_{0.3}MnO_3$ with FM insulating ground state in bulk form and also in previous works, e.g., in a detailed study on the cluster glass $Fe_{0.25}TiS_2$ by Koyano *et al.*[22] It is worth mentioning that the lower maximum in the ac susceptibility lies approximately in the same temperature region as the low temperature shoulder on the distribution function $f(T_B)$ (Fig. 6). As concerns $La_{0.5}Ca_{0.5}MnO_3$, the absolute value of the ac susceptibility peak is about 40 times larger compared to the $Pr_{0.5}Ca_{0.5}MnO_3$ nanocrystals. A more detailed analysis of the dynamical properties in the $Pr_{0.5}Ca_{0.5}MnO_3$ and $La_{0.5}Ca_{0.5}MnO_3$ nanocrystals will be presented in a separate paper.

Finally, let us discuss the properties of the "nearly FM" $La_{0.5}Ca_{0.5}MnO_3$ sample, using the FM metallic manganites $La_{0.75}Sr_{0.25}MnO_3$ as reference samples. It will be shown that the reduced moment of the nanoparticles and absence of saturation even in very high fields can be understood within the core-shell model. The relevant data are summarized in Fig. 9. It is seen that the dc susceptibility of nanoparticles $La_{0.5}Ca_{0.5}MnO_3$ (25 nm size) and $La_{0.75}Sr_{0.25}MnO_3$ (33 nm size) increases below T_C gradually, which is in contrast to the steplike increase for the typical FM bulk material $La_{0.75}Sr_{0.25}MnO_3$. The specific feature of the nanosize manganites is also large low-temperature coercivity demonstrated in the magnetization loops (see the right panel of Fig. 9). This is characteristic for the absence of domain walls in the nanocrystals—the FM core can be regarded as a single domain. Concerning the incomplete magnetization, we note that the sample $La_{0.75}Sr_{0.25}MnO_3$ of 33 nm particle size shows in the applied field of 70 kOe a nonsaturated moment of $2.92\mu_B$ per Mn at 5 K, irrespective of the ZFC or FC regime used in the experiment. In contrast, the full theoretical moment of $3.75\mu_B$ per Mn is easily obtained in bulk material. The moment reduction by 22% observed in the nanoparticles yields an estimate that the nonmagnetic surface layer is of thickness 1.5 nm. This value can be compared with the thickness 2.5–3.5 nm reported for the $La_{0.75}Sr_{0.25}MnO_3$ samples with particle sizes between 50 and 20 nm on the basis of the room-temperature magnetization data.[13] The surface layer in the less conducting $La_{0.5}Ca_{0.5}MnO_3$ system can be thicker, which may account for the large moment reduction 50–60 % in the 25 nm particles.

The nonmagnetic shell seems to be general property of magnetic nanoparticles. The extreme resistance of the shell to strong external field is reported, e.g., for the ferrite nanoparticles with spinel structure (see, e.g., Refs. 23–25). Since their ferrimagnetic ordering is driven by the superexchange

interactions that do not involve real electron transfer, the nature of the "magnetically dead" shell remains a controversial issue. On the other hand, the existence of nonmagnetic shell in the perovskite manganites is most likely intrinsic. We note that there is indeed an experimental evidence of weakening of the double exchange close to the surface—the relevant NMR study of the $La_{0.75}Sr_{0.25}MnO_3$ nanoparticles reports FM metallic phase in the core and FM insulating phase closer to the particle surface.[14] We expect that the e_g electron itinerancy which is at the root of the double exchange mechanism of the FM state is completely hindered at the outmost shell. To estimate the robustness of this nonmagnetic shell, we refer to the theoretical *t-J* model, applied by Venketeswara Pai[26] for the doped manganites. It is based on the effective Hamiltonian

$$H = J_{\mathrm{AF}} \sum_{\langle ij \rangle} S_i \cdot S_j - J_H \sum_{i,\alpha,\mu,\mu'} S_i c^{+}_{i\alpha\mu} \sigma_{\mu\mu'} c_{i\alpha\mu'} - \sum_{\langle ij \rangle,\mu} t^{\alpha\beta}_{ij} c^{+}_{i\alpha\mu} c_{j\beta\mu},$$

where $t \sim 0.15$ eV is the transfer integral that controls FM interactions mediated by itinerant e_g electrons, J_{AF} is the parameter of AFM superexchange between the local t_{2g} spins ($J_{\mathrm{AF}} S^2 \sim 8$ meV) and $J_H \sim 0.75$ eV gives an intrasite (Hund) interaction between the t_{2g} and e_g electrons. When the parameter t is largely reduced close to the nanoparticle surface, the superexchange interactions stabilize the AFM ordering in the particle shell. Applying the formula for perpendicular susceptibility $\chi_{\perp}$ of antiferromagnet with $J_{\mathrm{AF}} S^2 \sim 8$ meV, we obtain an estimate that the relatively large external field of 70 kOe induces a magnetization of about $0.25 \mu_{\mathrm{B}}$ per Mn only, which is indeed close to the paraprocess actually observed for 25 nm particles $La_{0.5}Ca_{0.5}MnO_3$ with large fraction of the surface phase (see the data at 5 K in the right panel of Fig. 5).

V. CONCLUSIONS

The present study has been undertaken with the aim to elucidate the suppression of charge ordering in the nanoparticles of half-doped manganites $Pr_{0.5}Ca_{0.5}MnO_3$ and $La_{0.5}Ca_{0.5}MnO_3$ and to characterize their magnetic state. The investigation shows that the room-temperature crystal structure as concerns the lattice distortion, Mn-O bonding lengths, and tilting of the MnO_6 octahedra does not change substantially with reducing grain size. This finding is coherent with reports on the comparable lattice parameters in nanoparticles and bulk of the some related manganite systems[10,21,27] and makes the speculations about the role of surface tension on the structure and physical properties of nanoparticles doubtful.

At low temperatures, no structural distortion, characteristic for (long- or short-range) charge ordering is observed on the 25 nm particles, which is in striking distinction with behavior of bulk samples. Consistently, there are also missing anomalies in the temperature dependence of magnetic susceptibility, which generally accompany the charge-ordering transition at T_{CO} and onset of the CE-type AFM arrangement at T_{N}. In the case of $La_{0.5}Ca_{0.5}MnO_3$, the neutron-diffraction and magnetic experiments confirm a formation of stable FM state in the nanoparticles, which points to a dominance of the double exchange interactions in this system. On the other hand, the spontaneous formation of FM state detected in $Pr_{0.5}Ca_{0.5}MnO_3$ involves only a minor part of the nanoparticles while most of the system can be characterized as a charge and orbital glass with random magnetic correlations between frozen spins. Nevertheless, a global FM state can be induced by applying of external field of few tens kilooersted.

Since the occurrence of FM state in the nanosize $Pr_{0.5}Ca_{0.5}MnO_3$ is limited and arises at rather low temperature 100 K, i.e., well below $T_{\mathrm{CO}} = 245$ K for the bulk, it arises naturally a question why charge order is not established in the particles. In our opinion, the absence of the charge-ordering transition should be ascribed to surface effects solely. As pointed out in Ref. 4, the charge ordering in bulk material originates from a soft mode and develops through noncommensurate configurations before reaching the ideal superstructure corresponding to the Mn^{3+}/Mn^{4+} ratio of 1:1 (see also Ref. 17). We suggest that this process is hindered in nanocrystals due to pinning of discommensurations to the surface of grains. The stable long-range ordering is thus inaccessible.

The situation for the 25 nm particles of $La_{0.5}Ca_{0.5}MnO_3$ is different. The spontaneous FM ordering occurs below $T_{\mathrm{C}} = 260$ K, which is notably higher than the charge-ordering temperature $T_{\mathrm{CO}} = 225$ K for the bulk material. The formation of the charge-order state is thus improbable. Nevertheless, the saturated FM state is not achieved because of the magnetic core—nonmagnetic shell structure of the nanoparticles. We consider that the surface shell consists of Mn ionic spins that are strongly AFM coupled due to a dominance of the superexchange interactions over the double exchange ones close to the particle surface.

ACKNOWLEDGMENTS

This study was performed under the support of the Academy of Sciences of the Czech Republic (Project No. KAN200200651). The neutron-diffraction experiments were supported by the Ministry of Education, Youth and Sports (Project No. MSM6840770021).

*Corresponding author; jirak@fzu.cz

[1] J. B. Goodenough, Phys. Rev. **100**, 564 (1955).
[2] P. G. Radaelli, D. E. Cox, M. Marezio, and S.-W. Cheong, Phys. Rev. B **55**, 3015 (1997).
[3] E. Pollert, S. Krupicka, and E. Kuzmicova, J. Phys. Chem. Solids **43**, 1137 (1982).
[4] Z. Jirák, F. Damay, M. Hervieu, C. Martin, B. Raveau, G. Andre, and F. Bouree, Phys. Rev. B **61**, 1181 (2000).
[5] M. Tokunaga, N. Miura, Y. Tomioka, and Y. Tokura, Phys. Rev. B **57**, 5259 (1998).
[6] S. Mori, C. H. Chen, and S.-W. Cheong, Phys. Rev. Lett. **81**, 3972 (1998).
[7] P. G. Radaelli, D. E. Cox, M. Marezio, S.-W. Cheong, P. E. Schiffer, and A. P. Ramirez, Phys. Rev. Lett. **75**, 4488 (1995).
[8] Q. Huang, J. W. Lynn, R. W. Erwin, A. Santoro, D. C. Dender, V. N. Smolyaninova, K. Ghosh, and R. L. Greene, Phys. Rev. B **61**, 8895 (2000).
[9] R. S. Freitas, L. Ghivelder, P. Levy, and F. Parisi, Phys. Rev. B **65**, 104403 (2002).
[10] E. Rozenberg, M. I. Tsindlekht, I. Felner, E. Sominski, A. Gedanken, Ya. M. Mukovskii, and Cheol Eui Lee, IEEE Trans. Magn. **45**, 2576 (2009).
[11] T. Zhang and M. Dressel, Phys. Rev. B **80**, 014435 (2009).
[12] K. Shantha Shankar, S. Kar, G. N. Subbanna, and A. K. Raychaudhuri, Solid State Commun. **129**, 479 (2004).
[13] S. Vasseur, E. Duguet, J. Portier, G. Goglio, S. Mornet, E. Hadova, K. Knizek, M. Marysko, P. Veverka, and E. Pollert, J. Magn. Magn. Mater. **302**, 315 (2006).
[14] D. Rybicki, M. Sikora, Cz. Kapusta, P. C. Riedi, Z. Jirak, K. Knizek, M. Marysko, E. Pollert, and P. Veverka, Phys. Status Solidi C **3**, 155 (2006).
[15] T. Sarkar, B. Ghosh, A. K. Raychaudhuri, and T. Chatterji, Phys. Rev. B **77**, 235112 (2008).
[16] A. Daoud-Aladine, J. Rodríguez-Carvajal, L. Pinsard-Gaudart, M. T. Fernández-Díaz, and A. Revcolevschi, Phys. Rev. Lett. **89**, 097205 (2002).
[17] Z. Jirák, C. Martin, M. Hervieu, and J. Hejtmánek, Appl. Phys. A: Mater. Sci. Process. **74**, S1755 (2002).
[18] J. J. Lu, H. Y. Deng, and H. L. Huang, J. Magn. Magn. Mater. **209**, 37 (2000).
[19] P. Tartaj, T. Gonzalez-Carreno, O. Bomati-Miguel, C. J. Serna, and P. Bonville, Phys. Rev. B **69**, 094401 (2004).
[20] The Pr^{3+} paramagnetic contribution for $T>100$ K can be approximated by the effective magnetic moment $\mu_{\mathrm{eff}}(Pr^{3+}) \sim 3.41\mu_{\mathrm{B}}$, see K. Sekizawa, M. Kitagawa, and Y. Takano, J. Magn. Magn. Mater. **177-181**, 541 (1998). The value reflects the crystal field in perovskite-type oxides and is accidentally close to the free ion value $g_J\sqrt{J(J+1)}=3.58\mu_{\mathrm{B}}$.
[21] E. Rozenberg, M. I. Tsindlekht, I. Felner, E. Sominski, A. Gedanken, and Ya. M. Mukovskii, IEEE Trans. Magn. **43**, 3052 (2007).
[22] M. M. Koyano, M. Suezawa, H. Watanabe, and M. Inoue, J. Phys. Soc. Jpn. **63**, 1114 (1994).
[23] R. H. Kodama, A. E. Berkowitz, E. J. McNiff, and S. Foner, J. Appl. Phys. **81**, 5552 (1997).
[24] B. Martínez, X. Obradors, Ll. Balcells, A. Rouanet, and C. Monty, Phys. Rev. Lett. **80**, 181 (1998).
[25] H. R. Rechenberg, E. C. Sousa, J. Depeyrot, M. H. Sousa, R. Aquino, F. A. Tourinho, and R. Perzynski, Hyperfine Interact. **184**, 9 (2008).
[26] G. Venketeswara Pai, Phys. Rev. B **63**, 064431 (2001).
[27] S. S. Rao, S. Tripathi, D. Pandey, and S. V. Bhat, Phys. Rev. B **74**, 144416 (2006).